arXiv:astro-ph/0303304v1 13 Mar 2003

Halo properties in models with dynamical Dark Energy

A. Klypin
Astronomy Department, New Mexico State University, Box 30001, Department 4500, Las Cruces, NM 88003-0001

A.V. Macciò, R. Mainini & S.A. Bonometto
Physics Department G. Occhialini, Università degli Studi di Milano–Bicocca, Piazza della Scienza 3, I20126 Milano (Italy)
I.N.F.N., Via Celoria 16, I20133 Milano (Italy)

ABSTRACT

We study properties of dark matter halos in a variety of models which include Dark Energy (DE). We consider both DE due to a scalar field self–interacting through Ratra–Peebles or SUGRA potentials, and DE with constant negative $w = p/\rho > -1$. We find that at redshift zero the nonlinear power spectrum of the dark matter, and the mass function of halos, practically do not depend on DE state equation and are almost indistinguishable from predictions of the ΛCDM model. This is consistent with the nonlinear analysis presented in the accompanying paper. It is also a welcome feature because ΛCDM models fit a large variety of data. On the other hand, at high redshifts DE models show substantial differences from ΛCDM and substantial differences among themselves. Halo profiles differ even at $z = 0$. DE halos are denser than ΛCDM in their central parts because the DE halos collapse earlier. Nevertheless, differences between the models are not so large. For example, the density at 10 kpc of a DE $\sim 10^{13}\mathrm{M}_\odot$ halo deviates from ΛCDM by not more than 50 %. This, however, means that DE is not a way to ease the problem with cuspy dark matter profiles. Addressing another cosmological problem - abundance of subhalos – we find that the number of satellites of halos in various DE models does not change relative to the ΛCDM, when normalized to the same circular velocity of the parent halo. To summarize, the best way to find which DE model fits the observed Universe is to look for evolution of halo properties. For example, the abundance of galaxy groups with mass larger than $10^{13}h^{-1}\mathrm{M}_\odot$ at $z \gtrsim 2$ can be used to discriminate between the models, and, thus, to constrain the nature of DE.

Subject headings: methods: analytical, numerical – galaxies: clusters – cosmology: theory – dark energy

1. Introduction

Mounting observational evidence for Dark Energy (Perlmutter et al. 1999; Riess et al. 1998; Tegmark, Zaldarriaga, & Hamilton 2001; Netterfield et al. 2002; Pogosian, Bond, & Contaldi 2003; Efstathiou et al. 2002; Percival et al. 2002; Spergel et al 2003), which probably contributes $\sim 70\%$ of the critical density of the Universe, rises a number of questions regarding consequences for galaxy formation. Traditionally, DE is described by the parameter $w = p/\rho$ characterizing its equation of state. The ΛCDM model ($w = -1$) was extensively studied during the last decade. Models with a constant negative $w > -1$ were much less studied, let alone physically motivated models with variable w (Mainini, Macciò, & Bonometto 2003; Mainini et al. 2003), for which no N–body simulation has been performed yet. Observations (Spergel et al 2003; Schuecker et al. 2003) limit the present day value of $w \lesssim -0.8$, though the limit has been derived for constant–w models only.

In the accompanying paper (Mainini et al. 2003) we describe procedures and give approximations for different quantities encountered in the linear and nonlinear analyzes of fluctuations in models in which DE is produced by a self–interacting scalar field (dynamical DE). In this paper we use these approximations to perform N–body simulations of models with dynamical DE and to study different properties of dark matter halos in such $N-$body simulations. For completeness we also study models with constant $w = -0.6$ and $w = -0.8$

Our main interest is in the models with varying w. These models use physically motivated potentials of scalar field and admit tracker solutions. We focus on the two most popular variants of dynamical DE (Wetterich 1988; Ratra & Peebles 1988; Wetterich 1995). The first model was proposed by Ratra & Peebles (1988, RP hereafter). It produces rather slow evolution of w. The second model (Brax & Martin 1999; Brax, Martin, & Riazuelo 2000; Brax & Martin 2000) is based on simple potentials in supergravity (SUGRA). It results in much faster evolving w. Hence, RP and SUGRA potentials cover a large spectrum of evolving w. These potentials are written as

$$V(\phi) = \frac{\Lambda^{4+\alpha}}{\phi^\alpha} \qquad RP, \tag{1}$$

$$V(\phi) = \frac{\Lambda^{4+\alpha}}{\phi^\alpha} \exp(4\pi G\phi^2) \quad SUGRA. \tag{2}$$

Here Λ is an energy scale, currently set in the range 10^2–10^{10} GeV, relevant for fundamental interaction physics. The potentials depend also on the exponent α. The parameters Λ and α define the DE density parameter Ω_{DE}. However, we prefer to use Λ and Ω_{DE} as independent parameters. Figure 10 in Mainini et al. (2003) gives examples of w evolution for RP and SUGRA models. The RP model considered in this paper has $\Lambda = 10^3$ GeV. At redshift $z = 0$ it has $w = -0.5$. The value of w gradually changes with the redshift: at $z = 5$ it is close to -0.4. The SUGRA model has $w = -0.85$ at $z = 0$, but w drastically changes with redshift: $w \approx -0.4$ at $z = 5$. Although the w interval spanned by the RP model covers values significantly above -0.8 (not favored by observations), this case is still important both as a limiting reference case and to emphasize that models with constant w and models with variable w produce different results even if average values of w are not much different. Constant w models have no physical motivation and can only be justified as toy models to explore the parameter space. The typical values of w observed in dynamical DE models, however, suggest to use $w = -0.8$ and $w = -0.6$ for the models with constant w.

2. Simulations

The Adaptive Refinement Tree code (ART; Kravtsov, Klypin & Khokhlov 1997) was used to run the simulations. The ART code starts with a uniform grid, which covers the whole computational box. This grid defines the lowest (zeroth) level of resolution of the simulation. The standard Particles-Mesh algorithms are used to compute density and gravitational potential on the zeroth-level mesh. The ART code reaches high force resolution by refining all high density regions using an automated refinement algorithm. The refinements are recursive: the refined regions can also be refined, each subsequent refinement having half of the previous level's cell size. This creates a hierarchy of refinement meshes of different resolution, size, and geometry covering regions of interest. Because each individual cubic cell can be refined, the shape of the refinement mesh can be arbitrary and match effectively the geometry of the region of interest.

The criterion for refinement is the local density of particles: if the number of particles in a mesh cell (as estimated by the Cloud-In-Cell method) exceeds the level $n_{\rm thresh}$, the cell is split ("refined") into 8 cells of the next refinement level. The refinement threshold may depend on the refinement level. The code uses the expansion parameter a as the time variable. During the integration, spatial refinement is accompanied by temporal refinement. Namely, each level of refinement, l, is integrated with its own time step $\Delta a_l = \Delta a_0/2^l$, where Δa_0 is the global time step of the zeroth refinement level. This variable time stepping is very important for accuracy of the results. As the force resolution increases, more steps are needed to integrate the trajectories accurately. Extensive tests of the code and comparisons with other numerical N-body codes can be found in Kravtsov (1999) and Knebe et al. (2000). The code was modified to handle DE of different types.

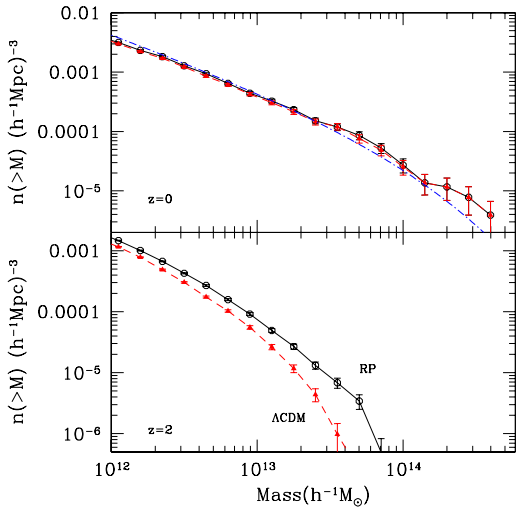

Fig. 1.— The mass function of isolated halos in the ΛCDM and RP models. The masses are found within virial radii. Results of all the rest of the models are in between these two models. At $z = 0$ there is no difference between the mass functions. The dot-dashed curve shows ST prediction. At $z = 2$ the mass functions of $w \neq -1$ models are above that of the ΛCDM.

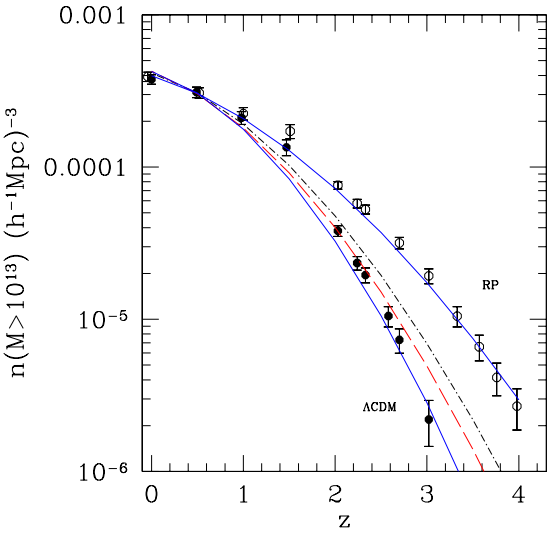

Fig. 2.— The evolution of the number density of halos with virial mass larger than $10^{13}h^{-1}$Mpc for different models. The bottom and top symbols are for $N-$body results in ΛCDM and in RP models. The curves show ST approximations. The dashed (dot-dashed) curve is for $w = -0.6$ (SUGRA) models. There is hardly any difference between models at redshifts smaller than $z = 1$. At higher z the number of halos in ΛCDM declines faster than for other models.

A large number of simulations were performed. The simulations have different sizes of computational box, different force and mass resolutions. Table 1 lists parameters of all our simulations. This large set of simulations allows us to study properties of halos ranging from dwarf satellites to clusters of galaxies. All simulations were extensively studied. We find that in all cases the results are bracketed by the ΛCDM and the RP models. Normally, differences between models are not very large. In order to avoid too crowded plots, in most of the presented plots we show only results of these two models.

3. Statistics of halos: power spectrum, mass and velocity functions

Figure 1 shows the mass function for isolated halos in the RP and the ΛCDM models. The simulations have the same initial phases and the same value $\sigma_8 = 0.75$. Thus, the differences between models are only due to different $w(t)$. Remarkably, at $z = 0$ the mass functions are practically indistinguishable: a mass function has no "memory" of the past evolution. In this figure we show only two models, but all other models show the same results at $z = 0$. The mass function is well fitted by the approximation provided by Sheth & Tormen (ST, Sheth & Tormen 1999; Sheth, Mo & Tormen 2001; Sheth & Tormen 2002).

At higher redshifts the situation is quite different: mass functions deviate substantially. Bottom panel in Figure 1 clearly demonstrates this: the number of clusters with mass large than $\approx 3 \times 10^{13}h^{-1}M_\odot$ is almost ten times larger in the RP simulation. The differences depend on mass. They are larger for massive clusters and much smaller for less massive halos. For galaxy-size halos with mass $\sim 10^{12}h^{-1}$M$_\odot$ the differences are only $\sim 20\%$, which will be difficult to detect observationally.

The dependence of halo abundance with redshift is further illustrated in Figure 2, where we study halos with mass of a group of galaxies. There is almost no way to distinguish models at

TABLE 1
PARAMETERS OF SIMULATIONS

Model	σ_8	Box size (h^{-1}Mpc)	Number of particles	Mass resolution ($h^{-1}M_\odot$)	Force resolution (h^{-1}kpc)
$w=-0.6$	0.75	80	128^3	2.0×10^{10}	5
$w=-0.8$	0.75	80	128^3	2.0×10^{10}	5
RP	0.75	60	128^3	8.4×10^{9}	5
	0.75	80	128^3	2.0×10^{10}	5
	0.75	160	256^3	2.0×10^{10}	10
	0.75	80	7.32×10^{5}	3.1×10^{8}	1.2
	1.00	60	7.32×10^{5}	1.3×10^{8}	0.9
SUGRA	0.75	60	128^3	8.4×10^{9}	5
	0.75	80	128^3	2.0×10^{10}	5
	0.75	160	256^3	2.0×10^{10}	5
ΛCDM	0.75	60	128^3	8.4×10^{9}	5
	0.75	80	128^3	2.0×10^{10}	5
	0.75	160	256^3	2.0×10^{10}	20
	0.75	80	7.32×10^{5}	3.1×10^{8}	1.2
	1.00	60	7.32×10^{5}	1.3×10^{8}	0.9

recent times $z<1$. But at $z=2-3$ the differences are quite significant. We note that observational detection of group-size halos at high redshifts is difficult, but feasible. We know how these objects should look like - almost the same as nearby groups. A group at high redshift should be more compact than a group at $z=0$ and it should consist of 3-10 Milky-Way size galaxies. Galaxies are expected to be distorted by interactions. A sample of few thousands galaxies can be used to count the number of groups. Comparison with the number of groups at present moment seems to be the way to discriminate between different models of DE.

For each halo we find the density profile and estimate the maximum circular velocity $V_{\rm circ}=\sqrt{GM(<r)/r}$. We then construct the circular velocity function of halos – the number density of halos with given $V_{\rm circ}$. The velocity function is a kin of the mass function, but it probes deeper inside halos. For a typical halo discussed here with a concentration $C\approx10$, the radius of the maximum circular velocity is about five times smaller than the virial radius. Figure 3 shows the velocity function at $z=2$ for RP and ΛCDM models. Just as

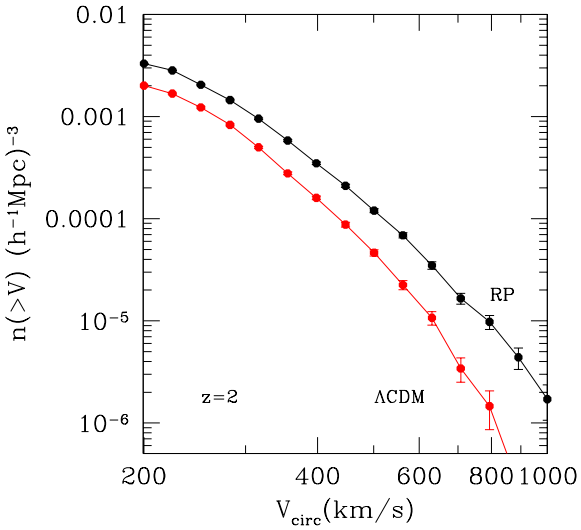

Fig. 3.— The number density of halos with the maximum circular velocity larger than $V_{\rm circ}$ at $z=2$. We show RP and ΛCDM models.

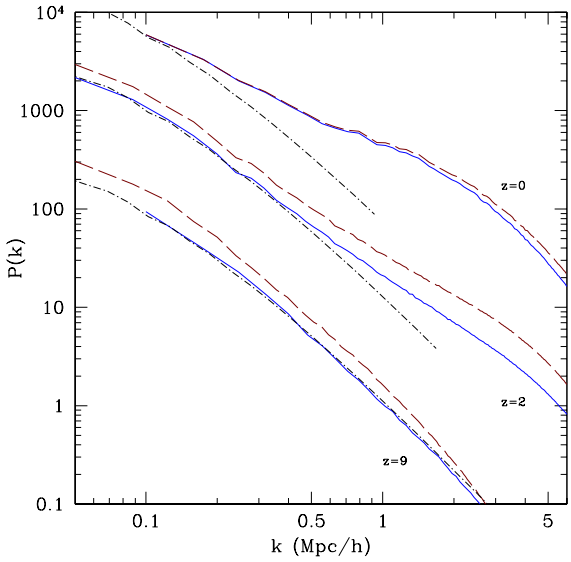

Fig. 4.— Power spectrum of fluctuations of dark matter for the ΛCDM (full curves) and for the RP (dashed curves) models at different redshifts. The dot-dashed curves show linear spectra for the ΛCDM model. At high redshifts fluctuations in the RP model are larger than for the ΛCDM model resulting in earlier collapse and in more dense halos. The differences in $P(k)$ are the largest at $z = 2 - 3$.

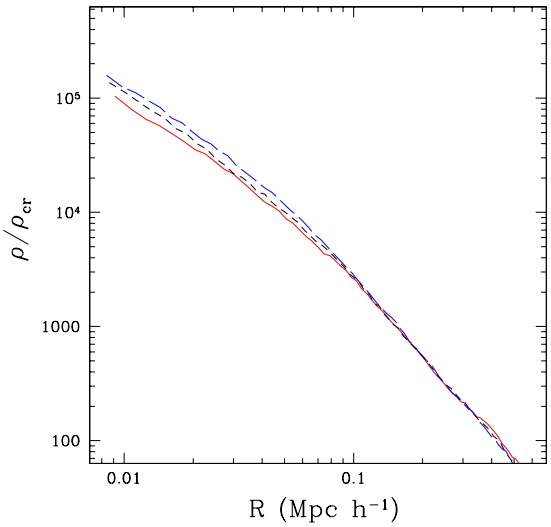

Fig. 5.— Profile of the same halo simulated in different models. The full curve is for the ΛCDM model. The shot (long) dashed curve is for SUGRA (RP) models. The halo has the virial mass $5 \times 10^{13} h^{-1}\mathrm{M}_\odot$. For different DE models the density profiles are practically the same in the outer $R > 100h^{-1}$kpc region. Each profile is well approximated by the NFW profile.

in the case of the mass function, the differences between models are larger at high redshifts. At given redshift the differences are larger for massive halos. Still, the velocity function brings new results. Even at $z = 2$ the mass functions are very close for low mass halos with virial mass $\approx 10^{12} h^{-1}\mathrm{M}_\odot$. These halos have $V_{\rm circ} \approx 200$ km/s. The velocity functions at that $V_{\rm circ}$ are visibly different: RP model has about 1.5 times more halos. The only way to explain this is to have more concentrated halos in RP model. In the next section we will explore this possibility in detail.

Figure 4 shows the evolution of the power spectrum $P(k)$ for fluctuations in the dark matter. The power spectrum basically follows the same pattern as the mass function: relatively large differences at high redshift, which become much smaller at $z = 0$. At $z = 0$ the deviations remain only on small scales ($k > 2$).

4. Halo structure

We start our study of halo profiles by making high resolution simulations of the same halo in different models. The halo was initially identified in a low resolution run. Short waves were added to the spectrum of initial perturbations and the halo was simulated again using $\approx 2 \times 10^5$ particles. In the ΛCDM model the halo has virial mass $5 \times 10^{13} h^{-1}\mathrm{M}_\odot$ and virial radius $730h^{-1}$kpc. It is accurately fitted by the NFW profile (Navarro, Frenk & White 2002) with the concentration $C_{\rm vir} = 7.2$. In the RP model the virial radius is $680h^{-1}$kpc – visibly smaller than for the ΛCDM halo. The RP halo also have larger maximum circular velocity as compared with the ΛCDM halo. Figure 5 shows profiles of the halo in the ΛCDM, RP, and SUGRA models. In spite of the fact that the virial radii for all the models are different, the density profiles in the outer part of the halo $R > 100h^{-1}$kpc are practically the same: from $100h^{-1}$kpc to $700h^{-1}$kpc the differences are less than 10%. The halos differ only in the central region $R < 100h^{-1}$kpc. The RP halo is clearly denser and more concentrated

than the ΛCDM halo with the SUGRA halo being in between. This difference can be used to discriminate between the models. Yet, it will not be easy because the differences are relatively small: factor 1.5 at $10h^{-1}$kpc.

The RP has a smaller virial radius because the virial radius in the RP model is defined at larger overdensity ($\Delta_{vir,RP} = 149.8\ \rho_{cr}$).This is the prediction of the top-hat model of halo collapse used to define the virial mass (Mainini et al. 2003). There is nothing wrong with it, but it complicates the comparison of density profiles and concentrations in different DE models. For example, a halo with exactly the same profile will have different virial radii and, thus, different concentrations in different DE models. In order to make comparison of density profiles less ambiguous, we decided to measure the halo concentration as the ratio of the radius at the overdensity of the ΛCDM model (103 times the critical density) to the characteristic ("core") radius of the NFW profile. The effect of using the radius at the constant overdensity instead of the virial radius is relatively small. For typical RP halo with virial mass $\sim 10^{13}h^{-1}\mathrm{M}_\odot$ the virial radius is $\sim 15\%$ smaller as compared with the constant overdensity radius.

We also study profiles of hundreds of halos in simulations with lower resolution. Figure 6 shows the dependence of halo concentration on the mass of halos in simulations with $80h^{-1}$Mpc box with $\sigma_8 = 0.75$. This plot shows the same tendency, which we found for the high-resolution halo: models with dynamical DE produce more concentrated halos. Figure 7 shows the distribution of halo concentrations for halos in mass range $(5-10)\times 10^{13}h^{-1}\mathrm{M}_\odot$. Halos with large deviations from NFW fits (non-relaxed halos) are not used. The spread of concentrations in the ΛCDM model is about twice smaller than in Bullock et al. (2001).

Abundance of subhalos in the ΛCDM model is a known problem (Klypin et al. 1999; Moore et al. 1999). It is interesting to find where dynamical DE models stand regarding the problem. Because fluctuations in dynamical DE models collapse earlier than in the ΛCDM model, one naively expects that the number of subhalos is also larger. We study the number of subhalos in a high resolution halo. The halo is simulated in the RP and the ΛCDM models. The halo with virial mass $2.4\times 10^{13}h^{-1}\mathrm{M}_\odot$ is resolved with particles of mass

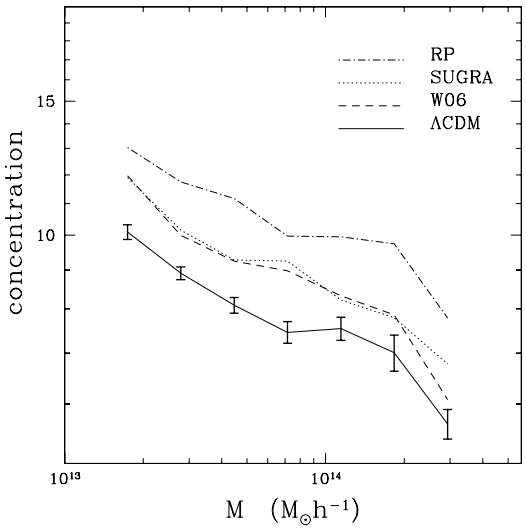

Fig. 6.— Dependence of concentration on halo mass. Halos for models with $w \neq -1$ are all more concentrated and, thus, are denser than the halos in the ΛCDM model. To avoid crowding we show statistical errors only for the ΛCDM model.

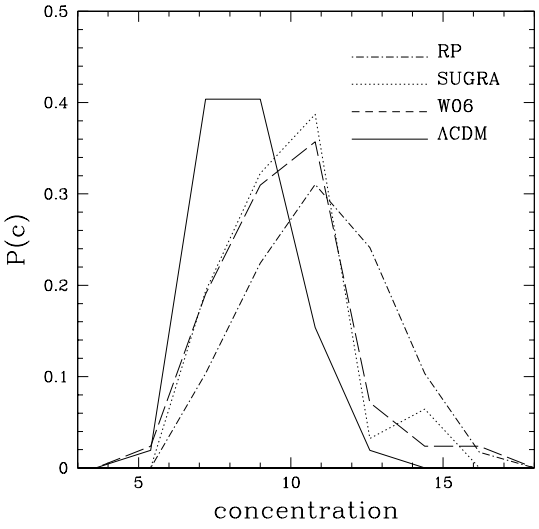

Fig. 7.— Distribution of halo concentrations for halos in mass range $(5-10)\times 10^{13}h^{-1}\mathrm{M}_\odot$ for different models. Halos with large deviations from NFW fits (non-relaxed halos) are not used.

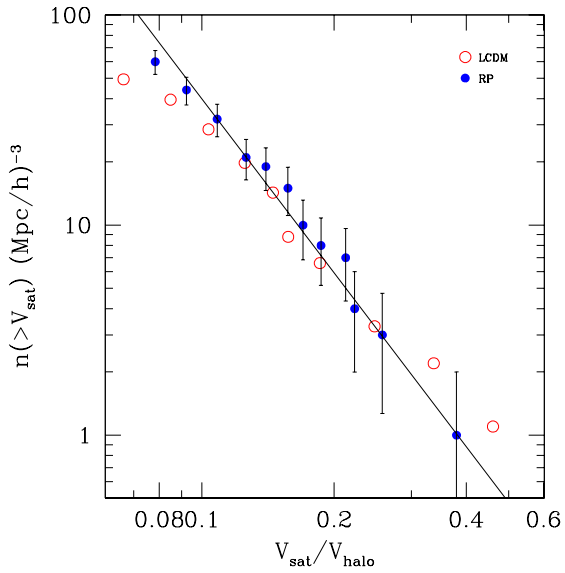

Fig. 8.— Abundance of subhalos in a halo with virial mass $M_{\rm vir} = 2.4 \times 10^{13} h^{-1}{\rm M}_\odot$. When normalized to the circular velocity of the parent halo, the velocity function is the same for both the RP and the ΛCDM models and is well approximated by the power-law $n(> V) \propto V^{-2.75}$. Vertical bars indicate the shot-noise errors.

$1.3 \times 10^8 h^{-1}{\rm M}_\odot$. The maximum circular velocity of the halo in ΛCDM (RP) model is 522 km/s (594 km/s). The force resolution $\approx 1 h^{-1}$kpc allows us to resolve dwarf DM halos with circular velocity larger than 30 km/s. For each (sub)halo we measure the density profile and estimate the value of the maximum circular velocity.

The number of subhalos in the RP halo is larger than in the ΛCDM halo: Inside the radius with the mean overdensity 103 of the critical density there are 87 satellites in the RP halo and 52 satellites in the ΛCDM model. Thus, there are a factor of 1.7 more satellites in the RP halo. Nevertheless, this large difference can be misleading because the circular velocity of the RP halo is larger by factor 1.14 and halos with larger circular velocity have a tendency to have more satellites (Klypin et al. 1999). In Figure 8 we plot the number of satellites as the function of the ratio of the satellite velocity to the halo velocity. Differences between the models are very small. It is also interesting to note that the velocity function of the subhalos is well approximated by the power-law $n(> V) \propto V^{-2.75}$. The slope of the power is the same as for subhalos of Milky Way-size halos (Klypin et al. 1999). In other words, it indicates that the slope does not depend on the mass of halo and does not depend on the DE equation of state.

5. Discussion and conclusions

Models with the dynamical DE are in infant state. We do not know the nature of DE. Thus, a great arbitrariness exists on the choice of the equation of state $w(t)$.

At first sight it seems that the situation is hopeless. This paper shows that this is not true: if we accept that w is close to -1 at $z = 0$, as many observations suggest, and that w monotonically increases with redshift, dynamical models are useful and can produce definite predictions for properties of halos and for galaxies hosted by the halos. Furthermore, the differences between rather extreme models of DE appear to be relatively small. In other words, one can make detailed predictions for properties of dark matter halos and for their clustering without knowing too many details of w evolution. Yet, the differences between models of DE exist and can be used to constrain the value and the evolution of w. In particular, distinguishing DE models by using only the value of w at the present time is clearly insufficient.

The main tendency, which we find in all DE models is that halos tend to collapse earlier. As the result, they are more concentrated and more dense in the inner parts. Nevertheless, differences are not so large. For example, the density at 10 kpc of a $\sim 10^{13}{\rm M}_\odot$ halo in a dynamical DE model deviates from ΛCDM not more than by 50 %. This, however, means that DE is not a way to ease the problem with cuspy dark matter profiles. Nevertheless, the differences in halo profiles can be exploited. Denser cluster profiles in dynamical DE models can be tested by both the weak (Bartelmann et al 2002) and especially by the strong gravitational lensing. Bartelmann et al (1998) and Meneghetti et al (2000) argue that the arclet statistics favors ΛCDM models when compared with the open CDM models. In this respect dynamical DE models are between the above two models. This problem deserves further investigation.

We find that the best way to find which DE

model fits the observed Universe best is to look for evolution of halo properties. For example, comparison of low- and high-z ($z \gtrsim 2$) abundances of galaxy groups with mass larger than $10^{13}h^{-1}\mathrm{M}_{\odot}$ can be used to discriminate between models. Potentially, clustering of galaxies at redshifts $2-3$ can also be used for this.

In this paper we mostly pay attention to the group-size halos with mass $\sim 10^{13}h^{-1}\mathrm{M}_{\odot}$ at high redshifts as a probe for the DE. In the accompanying paper Mainini et al. (2003) we also argue that abundance of clusters at intermediate redshifts can be used as a test for DE models. Available cluster samples, unfortunately, still include too few clusters at intermediate and high redshift.

To directly investigate the cluster mass function at intermediate redshift with optical instruments, deep optical or near infrared data are used. Exploiting this kind of data the Red–Sequence Cluster Survey (Gladders & Yee 2000) and the Las Campanas Distant Cluster Survey (Nelson et al. 2002) were compiled. Taking carefully in to account selections effects is rather hard and these samples include just tenth of objects. Selection effects are easier to handle for clusters detected in X–rays. The ROSAT data were used to compile a number of cluster catalogs (Ebeling et al. 1996, 2000; de Grandi et al. 1999). The most numerous sample of flux limited clusters (REFLEX: Guzzo et al 1999, Schuecker et al 2003b) is based on the ROSAT observations. It includes 426 objects with redshifts up to $z \sim 0.3$. The XMM Survey (Pierre 2000) will add another 800 clusters with redshifts up to $z \sim 1$. Hopefully, follow–up optical programs will provide redshifts for the clusters in the catalogs. While designed for different goals, REFLEX have been already used to constrain many cosmological parameters such as σ_8, and, together with SNIa data, it provides important constraints on the DE equation of state (Schuecker et al 2003a).

The Suniaev-Zeldovich (SZ) effect (scattering of CMB photons by the hot intracluster gas) is even more promising for detection of high–z clusters (La Roque et al, 2003; Weller et al 2002, Hu 2003). The shallow all-sky survey that the PLANCK experiment will produce will be supplemented by narrower surveys covering a smaller fraction of the sky, based on interferometric devices (OCRA: Browne et al 2000; SZA: Carlstrom et al 2000; AMIBA: Lo et al 2000; AMI: Kneisel 2001).

These new cluster catalogs require more extensive and detailed theoretical modeling. Confrontation of new observational data with theoretical predictions will be able to discriminate between different DE models.

In our analysis we also address another important issue: the abundance of subhalos. It is well known (Klypin et al. 1999; Moore et al. 1999) that in the ΛCDM model the number of predicted dwarf dark matter satellites significantly exceeds the observed number of satellite galaxies in the Local Group. There are different possibilities to explain this excess. The most attractive explanation is related with the reionization of the Universe resulting in heating of gas in dwarf halos, which prevents them from becoming galaxies (Bullock, Kravtsov, & Weinberg 2001,?; Somerville 2002; Benson et al. 2002).

We find that the number of satellites of halos, at $z = 0$, in various DE models does not change relative to the ΛCDM, when normalized to the same circular velocity of parent halo. If the reionization of the Universe is the solution of the problem, then the DE models predict an earlier reionization of the Universe, because the earlier collapse of dwarf dark matter halos requires an earlier reionization to avoid too many satellites at redshift zero. The recent WMAP results (Kogut et al 2003, Spergel et al 2003), can be interpreted as giving a large opacity for CMB photons $\tau \simeq 0.17 \pm 0.04$. If true, this requires that the reionization occurred at a redshift $z_{ri} \sim 13$–20, which is too large for the standard ΛCDM model (Gnedin 2000). If the early reionization happens in the ΛCDM model, it would predict too few satellites for the Local Group because too few dwarf halos collapse that early. Models with SUGRA DE seem to be in a better position to fit WMAP results and, at the same time, the observed number of satellites: in fact, in this model, halos collapse at higher redshifts as compared with the ΛCDM model.

ACKNOWLEDGEMENTS

We thank INAF for allowing us the CPU time to perform some of the simulations used in this work at the CINECA consortium (grant cnami44a on the SGI Origin 3800 machine).

REFERENCES

Bartelmann M., Huss A., Carlberg J., Jenkins A. & Pearce F. 1998, A&A 330, 1

Bartelmann M., Perrotta F. & Baccigalupi C. 2002, A&A 396, 21

Benson, A. J., Lacey, C. G., Baugh, C. M., Cole, S., & Frenk, C. S. 2002, MNRAS, 333, 156

Brat, P. & Martin, J., 1999, Phys.Lett., B468, 40

Brax, P. & Martin, J., 2000, Phys.Rev. D, 61, 103502

Brax P., Martin J. & Riazuelo A., 2000, Phys.Rev. D, 62, 103505

Browne, I.W., et al. in "Radio Telescopes" (SPIEProc. vol 41015) edited by H. R. Butcher (2000)

Bullock, J. S., Kravtsov, A. V., & Weinberg, D. H. 2000, ApJ, 539, 517

Bullock, J. S., Kravtsov, A. V., & Weinberg, D. H. 2001, ApJ, 548, 33

Bullock J., Kolatt T., Sigad Y., Somerville R., Kravtsov A., Klypin A., Primack J. & Dekel A. 2001, MNRAS, 321, 559

Carlstrom J.E., et al., in Constructing the Universe with Cluster of Galaxies, 2000, edited by F. Durret and G. Gerbal.

de Grandi et al., 1999, ApJ, 514, 148

Ebeling H., Voges W., Bohringer H., Edge A.C., Huchra J.P., Briel U.G., 1996, MNRAS, 281, 799

Ebeling H., Edge A.C., Allen S.W., Crawford C.S., Fabian A.C., Huchra J.P., 2000, MNRAS, 318, 333

Efstathiou, G. et al., 2002, MNRAS, 330, 29

Gladders, M.D. & Yee, H.K.C., 2000, AJ, 120, 2148

Gnedin, N. Y. 2000, ApJ, 535, 530

Guzzo L. et al 1999, The Messenger, 95, 27

Hu W., astro-ph/0301416,

Klypin A., Gottloeber S., Kravtsov A. & Khokhlov A. (1999) ApJ 516, 530

Klypin, A., Kravtsov, A. V., Valenzuela, O., & Prada, F. 1999, ApJ, 522, 82

Kneissl, R., et al., MNRAS. 2001, 328, 783

Kogut et al., 2003, astro–ph/0302213

Kravtsov A., Klypin A. & Khokhlov A., 1997 ApJ, 111, 73 K

La Roque S.J. et al., 2003, ApJ, 583, 559

Lo K.Y., et al., in New Cosmological Data and the values of the Fundamental Parameters, 2000, edited by A. Lasenby and A. Wilkinson.

Lokas, E.L., 2002, astro-ph/0112031

Mainini R., Macciò A.V. & Bonometto S.A., 2003, NewA 8, 172

Mainini R., Macciò A.V., Bonometto S.A., & Klypin, A., 2003

Meneghetti M., Bolzonella M., Bartelmann M., Moscardini L. & Tormen G. 2000, MNRAS 314, 338M

Moore, B., Ghigna, S., Governato, F., Lake, G., Quinn, T., Stadel, J., & Tozzi, P. 1999, ApJ, 524, L19

Navarro, J. F., Frenk, C.S. & White S.D.M., 1997, ApJ, 490, 493

Nelson A.E., Gonzalez A.H., Zaritsky D. & Dalcanton J.J, 2002, ApJ, 566, 103

Netterfield, C. B. et al. 2002, ApJ, 571, 604

Percival W.J. et al., 2002, astro-ph/0206256, MNRAS(in press)

Perlmutter S. et al., 1999, ApJ, 517, 565

Pierre M., 2000, astro-ph/0011166

Pogosian, D., Bond, J.R., & Contaldi, C. 2003, astro-ph/0301310

Ratra B., Peebles P.J.E., 1988, Phys.Rev.D, 37, 3406

Riess, A.G. et al., 1998, AJ, 116, 1009

Schuecker P., Caldwell R.R., Boehringer H., Collins C.A. & Guzzo L., 2003 astro-ph/0211480, A&A (in press)

Schuecker P., Bhringer H., Collins C.A. & Guzzo L., 2003, A&A, 398, 867

Sheth R.K., Mo H.J. & Tormen G., 2001, MNRAS, 323 ,1

Sheth R.K. & Tormen G., 1999, MNRAS, 308, 119

Sheth R.K. & Tormen G., 2002, MNRAS, 329, 61

Somerville, R. S. 2002, ApJ, 572, L23

Spergel et al. 2003, astro–ph/0302209

Tegmark, M., Zaldarriaga, M., & Hamilton, A. J. 2001, Phys. Rev. D, 63, 43007

Weller, J., Battye, R. & Kneissl, R. 2002, Phys.Rev.Lett., 88, 231301

Wetterich C., 1988, Nucl.Phys.B, 302, 668

Wetterich C., 1995 A&A 301, 32

This 2-column preprint was prepared with the AAS LaTeX macros v5.0.